224
9/5/81

ornl

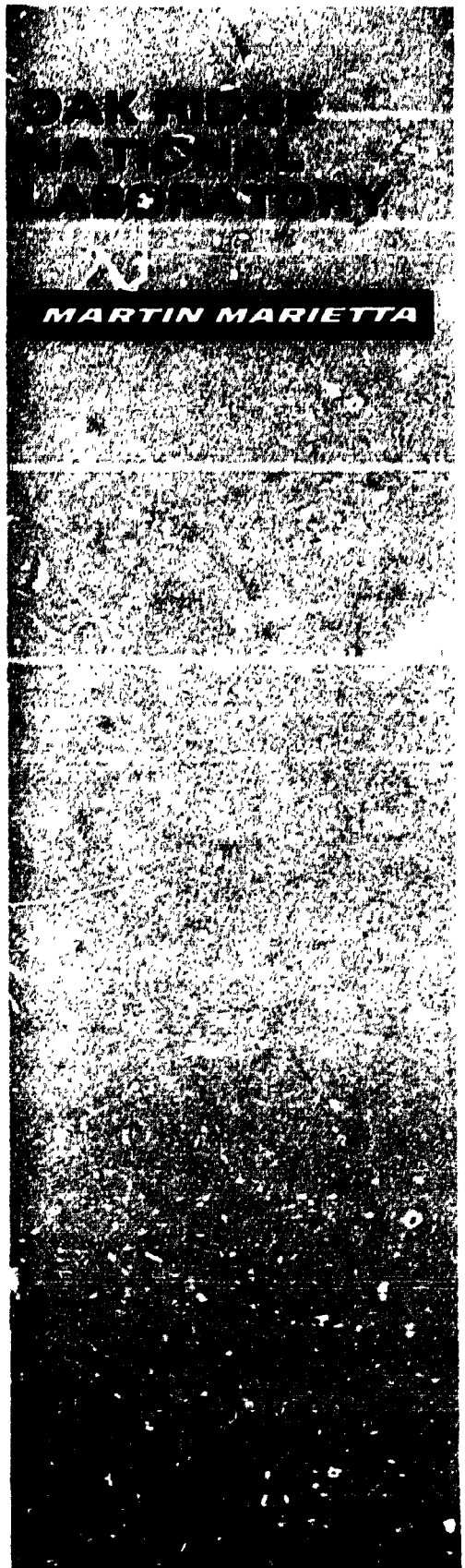

DR-0364-6

ORNL/TM-9128

I-16742

Comparison of Plasma Results in EBT-1 and NBT-1M

R. J. Colchin
J. C. Glowienka

ORNL/TM-9128
Dist. Category UC-20 f, g

Fusion Energy Division

COMPARISON OF PLASMA RESULTS IN EBT-1 AND NBT-1M

R. J. Colchin and J. C. Glowienka

ORNL/TM--9128

DE84 016573

Date Published: July 1984

DISCLAIMER

Prepared by the
OAK RIDGE NATIONAL LABORATORY
Oak Ridge, Tennessee 37831
operated by
Martin Marietta Energy Systems, Inc.
for the
U. S. DEPARTMENT OF ENERGY
under Contract No. DE-AC05-840R21400

CONTENTS

LIST OF FIGURES

LIST OF TABLES

ABSTRACT

Plasma results from the ELMO Bumpy Torus (EBT-1) and Nagoya Bumpy Torus (NBT-1M) experiments are compared. Both devices have 24 mirror field coils arranged to form a torus, and both use 18-GHz electron cyclotron resonance heating power. The main difference is that NBT-1M is somewhat (~30%) smaller than EBT-1. However, when plasma results are scaled to eliminate this size discrepancy, plasma results are found to be nearly equivalent in both bumpy tori.

1. INTRODUCTION

ELMO Bumpy Torus (EBT-1) and Nagoya Bumpy Torus (NBT-1M) are unique plasma devices that share a similar magnetic geometry, plasma heating source, and many similar diagnostics. They are somewhat different in size, but more importantly, they were built and are operated half a world apart.

EBT-1 is the older of the two devices, being first operated in 1973; NBT-1M began operation almost a decade later. Because the data base for EBT-1 was well established by the time NBT-1M was initiated, it was felt that NBT-1M experimental time could be more profitably used for new experiments, rather than systematically repeating the EBT-1 results. Also, the results have been continually refined on both devices as new diagnostics have been brought into use. There now exists a limited body of data common to both devices, and a detailed comparison of results (where possible) would appear to be in order. That is the purpose of this report.

2. SIZE COMPARISON

EBT-1 is described in refs. 1 and 2, and details of NBT-1M are given in ref. 3. Both devices have 24 magnetic mirror field coils, canted so as to form a torus. Both are heated by 18-GHz microwave power injected into multimode cavities. Both devices use hydrogen as the working gas.

One clear difference between NBT-1M and EBT-1 is that of size. A detailed comparison is given in Table 1, and the relative size of the cavities is shown in Fig. 1. Generally speaking, EBT-1 is about a third bigger than NBT-1M. This size difference comes about because the NBT-1M cavities were specifically designed so as to minimize surface plasma and, thus, funnel more of the microwave power into ring and core heating. Because NBT-1M additionally has a slightly smaller major radius, its mirror ratio is higher (i.e., 2.4 as contrasted with a mirror ratio of 1.9 for EBT-1). The size difference affects the microwave heating power density[3,4] (for equal input power into both devices).

3. PLASMA COMPARISON

Ideally, data comparisons should be made at identical microwave powers and identical pressures in each plasma device. It is sometimes possible to find cases in

which the applied microwave powers were similar. However, pressures are recorded somewhat differently on the two devices, so a machine-to-machine calibration must be made.

Pressure calibration in NBT-1M relies on that of the manufacturer of the ionization gauge tubes. The EBT-1 ionization tubes have recently been absolutely calibrated by means of a spinning-rotor-type gauge, whereupon it was found that the pressure readings were about 50% lower for nitrogen gas. To convert EBT-1 pressures to hydrogen equivalents, as in NBT-1M, it is necessary to multiply by 2.5. Figure 2 shows microwave interferometer $<n_e \ell>$ data from EBT-1 and NBT-1M. The shapes of both curves are remarkably similar. As would be expected, the EBT-1 data have larger absolute values than those of NBT-1M because of the longer plasma path length ℓ through the EBT-1 cavity. If the effective path length through the cavity is assumed to be that of a ring diameter (Table 1), then absolute densities can be obtained, as plotted in Fig. 3. In this figure it can be seen that density in NBT-1M is about 20% higher than that of EBT-1 at a fixed pressure. This difference might be expected, as the plasma density is found to scale as the square root of the applied microwave power.[5] If it is assumed that this scaling holds for the power density as well, then the densities of Fig. 3 can be normalized by multiplying by the square root of the plasma volume (Table 1). The results of this normalization are plotted in Fig. 4. The results again agree to within about 20%, which is within the uncertainty of the path length ℓ.

Since the densities are in reasonable agreement, one might expect that the density profiles would be similarly matched. Profiles were measured on EBT-1 by using a 9-channel microwave interferometer and by Abel inverting the results. Cylindrical symmetry was assumed. A more accurate point-by-point determination was carried out on NBT-1 by detecting excitation radiation from a 4-keV neutral lithium beam. This diagnostic is absolutely calibrated by measuring the signal from neutral gas scattering. Profiles are compared in Figs. 5-7. In Fig. 5 the pressures are somewhat different, while in Figs. 6 and 7 the pressures are the same for both devices. Because of differing machine size, radial dimensions have been normalized by the inside and outside ring radii (Table 2). Densities have been normalized to unity at the plasma center.

Despite the coarseness of the EBT-1 data, Figs. 5-7 show that the density profiles are very similar. Note that the central EBT-1 interferometer channel was anomalously high, which biases the EBT-1 data to lower values than those of NBT-1M.

The presence of a potential well is an important feature of bumpy tori, and data from heavy ion beam probes can be compared both on the basis of well depth and well size. The comparison of well depths is subject to definition (i.e., uncertainties as to the spatial locations from which the data are taken) and exact alignment of the heavy ion beam systems. Nonetheless, Fig. 8 shows excellent agreement between EBT-1 and NBT-1M for like ring locations.

Another measure of comparison is that of potential well size. Because of the difficulty of obtaining the large amount of data necessary for a two-dimensional plot, only one such plot was constructed for EBT-1 (Fig. 9). Two such plots exist for NBT-1M (Figs. 10 and 11). The EBT-1 plot was made at somewhat higher pressure than those of NBT-1M, and additional microwave heating power was employed (10.6 GHz for EBT-1 and 8.5 GHz, in Fig. 11, for NBT-1M). The fractions of the ring radius occupied by the last closed potential contour are 0.52, 0.71, and 0.74 for Figs. 9 through 11. Thus, it appears that potential well scale size may be somewhat different in these devices.

Electron temperatures in NBT-1M are determined by six separate measurements. Three involve spectroscopic line ratios, plasma conductivity is used in a fourth, and Thomson scattering is used in the fifth. Of these methods, Thomson scattering is the most trusted. As shown in Fig 12, all five methods give temperatures less than 100 eV, and temperatures decrease with increasing neutral pressure. The sixth method of determining electron temperature is by means of soft Xrays. Tail temperatures of 1 and 20 keV are observed.

Also plotted in Fig. 12 are Thomson scattering temperatures for the EBT-1 device with 40 kW of 18-GHz power and 6-10 kW of 10.6-GHz power. These temperatures fall in the same range as those of NBT-1M. Soft X-ray tail temperatures are measured to be 200 to 600 eV.

The relative values of the particle confinement time can be compared by calibrated measurements of the H_α radiation. These data are plotted in Fig. 13. Note that the microwave heating power levels were not equal for the two experiments. Also, there is the possibility of diminished sensitivity in the NBT-1M measurements due to a window coating, making an absolute τ_p comparison questionable. Still, the trends of both curves are qualitatively the same.

Impurities are low in both devices, primarily due to impurity lifetimes of less than 1 ms. Aluminum, oxygen, and carbon are the principal impurities in EBT-S, with aluminum being the most abundant ($n_{Al}/n_e < 10^{-3}$). There is somewhat less data on impurities in NBT-1M, but it is believed that oxygen is the main impurity.

The ultimate vacuum pressure (which is a measure of residual gas impurities) is $p_o < 10^{-7}$ torr in NBT-1M and $p_o < 5 \times 10^{-7}$ torr in EBT-1. In both machines, impurity radiation represents a negligible power loss.

Plasma fluctuations are qualitatively similar in EBT-1 and NBT-1M, although they differ somewhat in detailed behavior. Both have regimes in which low-frequency flute modes exist outside the rings. Drift modes also are found that can penetrate into the core plasma. At frequencies of $f = 1\text{-}2\ f_{ci}$, the hot electron interchange mode is observed near the T-M transition.[4,6] At still higher frequencies, an as yet unidentified mode appears in the range of 30 to 100 MHz. At about 3 GHz, plasma fluctuations have been noted in EBT-1 that are tentatively identified with the whistler instability.

Finally, a comparison of hot electron ring properties can be made. Table 2 gives a comparison of ring parameters in which there is very little difference between EBT-1 and NBT-1M. The ring densities and temperatures quoted in Table 2 are derived from hard X-ray data. A direct measurement of β was attempted on NBT-1M by measuring the Zeeman splitting of line emission from lithium atoms. This measurement gave an upper limiter of $\beta < 10\%$, which is lower than that obtained from the hard X-ray measurements.

Detailed studies of the ring position have been conducted in NBT-1M by a movable hard X-ray cannon, H_α emission, and skimmer probes. It is concluded that the rings exist at $\omega_\mu = 2\omega_{ce}$, a conclusion shared by analysis of EBT-1 data.

4. CONCLUSIONS

This report has compared detailed plasma properties in EBT-1 and NBT-1M. These comparisons include $n_e\ell$, $n_e(r)$, $\phi(r)$, T_e, τ_p, impurity levels, plasma fluctuations, and hot electron rings. Because NBT-1M is about one-third smaller in physical size than EBT-1, we have attempted to scale the results for comparison. The principal scaling parameter used was the size of the hot electron rings.

Where direct comparisons were possible, we generally found the results on both devices to coincide to within the error limits of the measurements. An apparent exception is the relative size of the potential well, with the closed potential surfaces of NBT-1M occupying a larger fraction of the ring radius than those of EBT-1. All in all, it is very gratifying to find that devices constructed and operated in different parts of the world can exhibit nearly identical results.

ACKNOWLEDGMENTS

We would like to thank members of the EBT-1 and NBT-1M staffs for supplying the data used in this report. We would particularly like to thank the NBT-1M staff for their kind hospitality during the writing of this report and for their patience in explaining their results.

REFERENCES

1. F. W. Baity, Jr. et al., *Summary of EBT-1 Experimental Results*, ORNL/TM-6457, Oak Ridge Natl. Lab, 1978.
2. J. C. Glowienka, "ELMO Bumpy Torus: An Alternate Concept to Tokamaks and Mirrors," *J. Vac. Sci. Technol.* **18**, 1088 (1981).
3. M. Fujiwara, H. Tsuchidate, T. Kamimura, and NBT Group, *NBT-1M Design Report*, IPPJ-579, Institute of Plasma Physics, Nagoya University, Nagoya, Japan, 1982.
4. *Annual Review*, Institute of Plasma Physics, Nagoya University, April 1982 - March 1983, pp. 84-101.
5. R. J. Colchin et al., "Plasma Properties in the ELMO Bumpy Torus," *Plasma Phys.* **25**, 597 (1983).
6. S. Hiroe et al., *Observation of Hot Electron Ring Instabilities in ELMO Bumpy Torus*, ORNL/TM-8874, Oak Ridge Natl. Lab., 1983.

TABLE 1. EBT-1 and NBT-1M size comparison

	EBT-1	NBT-1M
Cavity diameter, cm	50.8	30.6
Ring diameter, cm	29.2	15.5
Throat diameter, cm	22.2	13.9
Major radius, cm	152	140
Average plasma diameter, cm	11	7
Plasma volume, L	360	135
Mirror ratio	1.9	2.4
B(center), gauss	5000	4986
P_μ (18 GHz), kW	≤60	≤45 (pulsed)

TABLE 2. Comparison of ring parameters

	EBT-1	NBT-1M
T_e, keV	100–200	230
n_e, x 10^{11} cm^{-3}	1–4	1–3
β, %	<35	<30
Δ (ring thickness), cm	~3	~3.5
r (ring radius), cm	12 (outside) 15 (inside)	7 (outside) 8 (inside)
B_{res} ($\omega_\mu = 2\,\omega_{ce}$), gauss	3216	3216

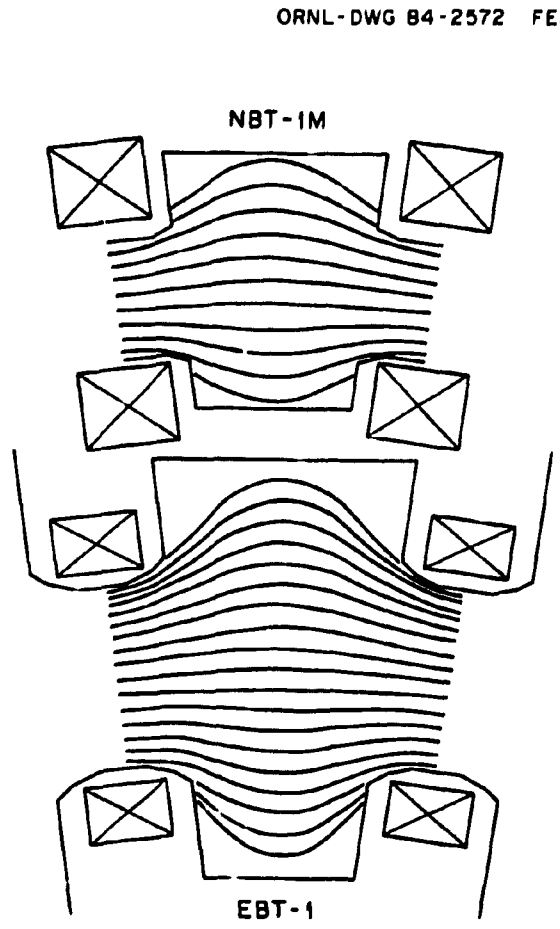

Fig. 1. Relative size comparison of NBT-1M and EBT-1 cavities. Field lines and coils are also shown.

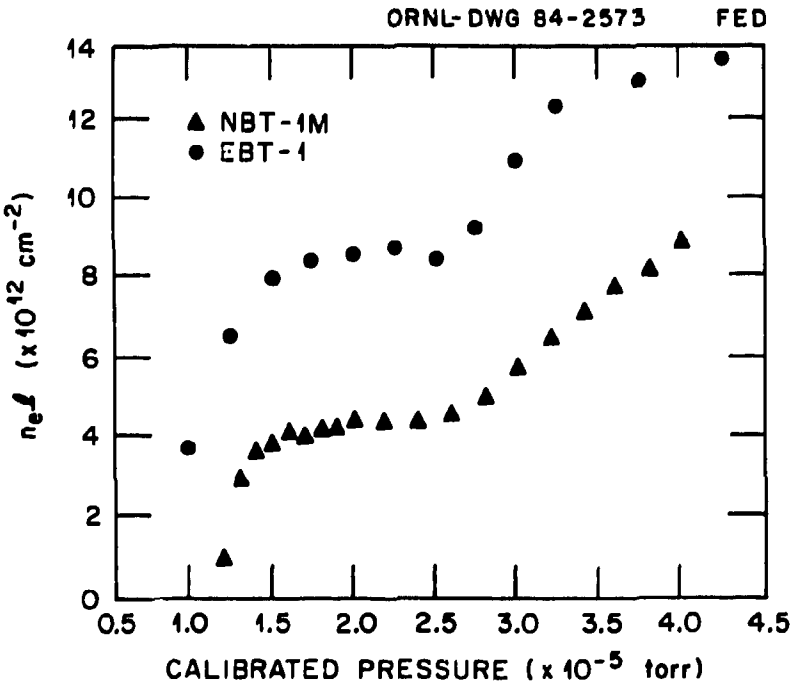

Fig. 2. $n_e\ell$ vs p_o comparison of EBT-1 and NBT-1M data. P_μ = 33 kW for NBT-1M and 30 kW for EBT-1.

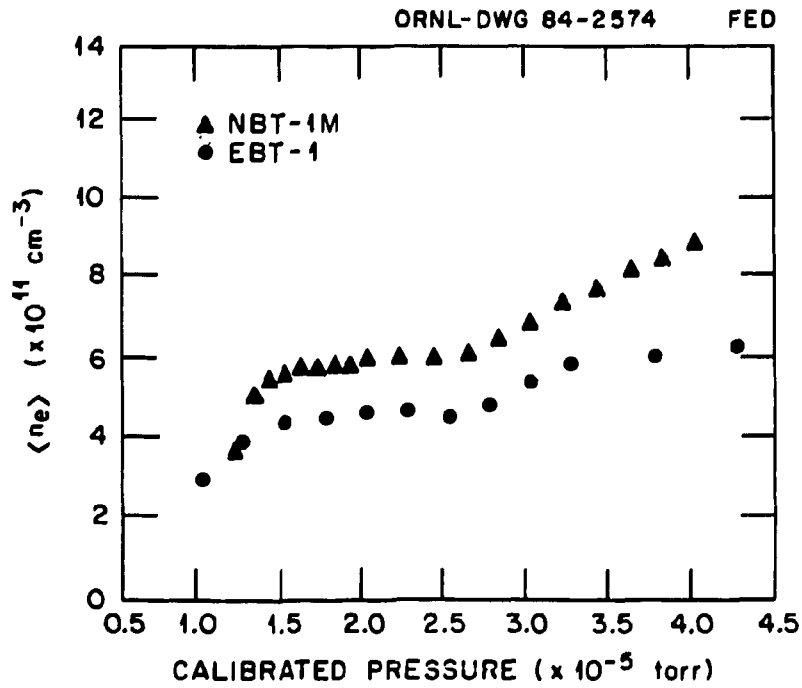

Fig. 3. Comparison of absolute densities obtained from the data of Fig. 2 divided by the ring diameters.

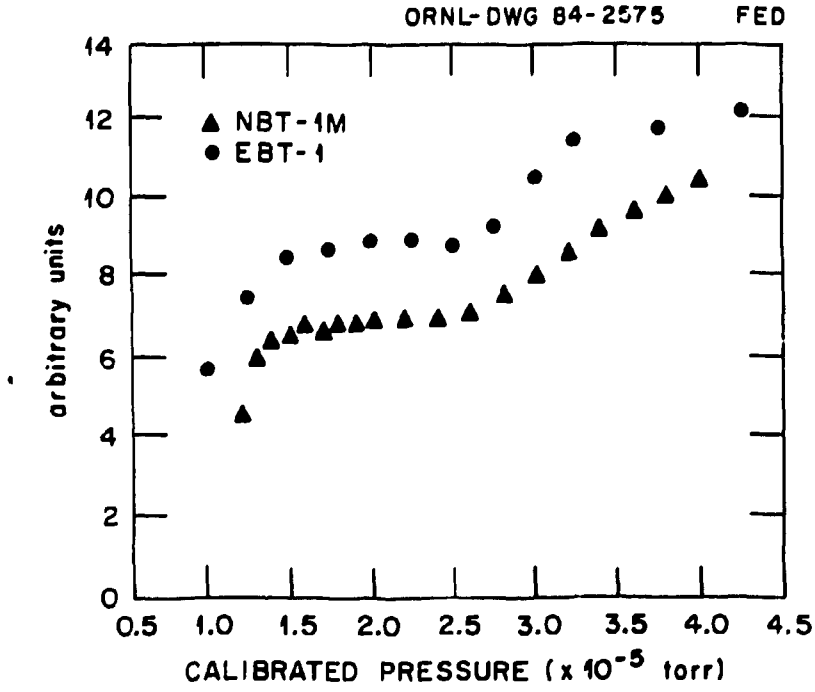

Fig. 4. Normalization of the densities of Fig. 3 by the inverse square root of the respective plasma volumes.

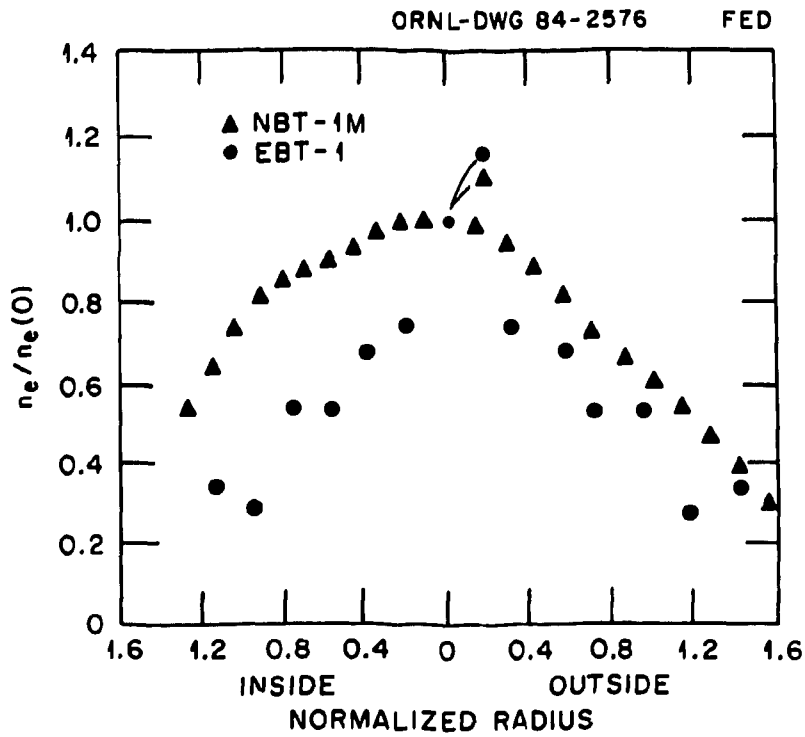

Fig. 5. Comparison of EBT-1 and NBT-1M density profiles. For EBT-1 p_o was 1.13×10^{-5} torr, which is near the T-M transition. For NBT-1M, $p_o = 1.5 \times 10^{-5}$ torr, which is in the mid T-mode. The applied microwave power levels were 40 and 30 kW for EBT-1 and NBT-1M, respectively.

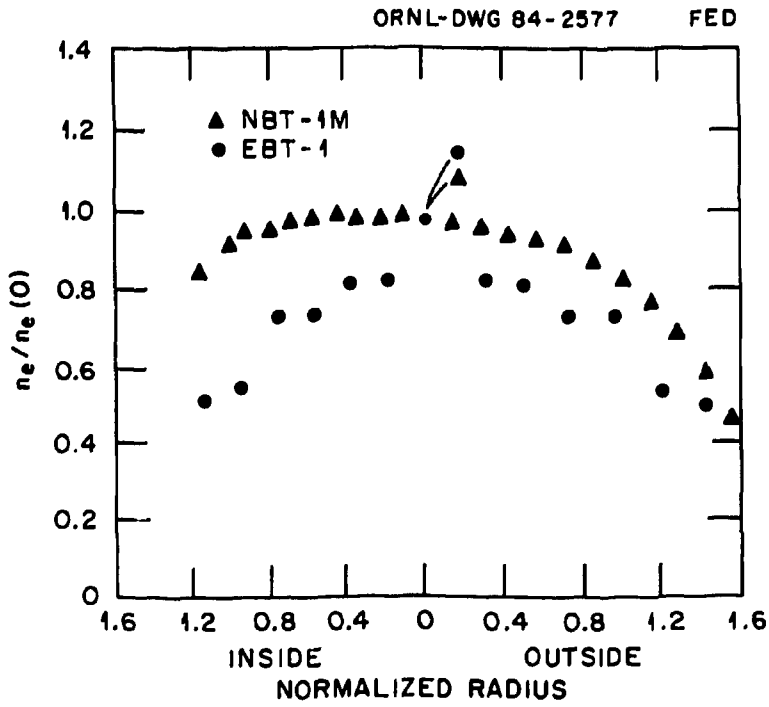

Fig. 6. Comparison of EBT-1 and NBT-1M density profiles at p_o = 2 x 10^{-5} torr, near the C-T transition. Applied microwave powers are the same as in Fig. 5.

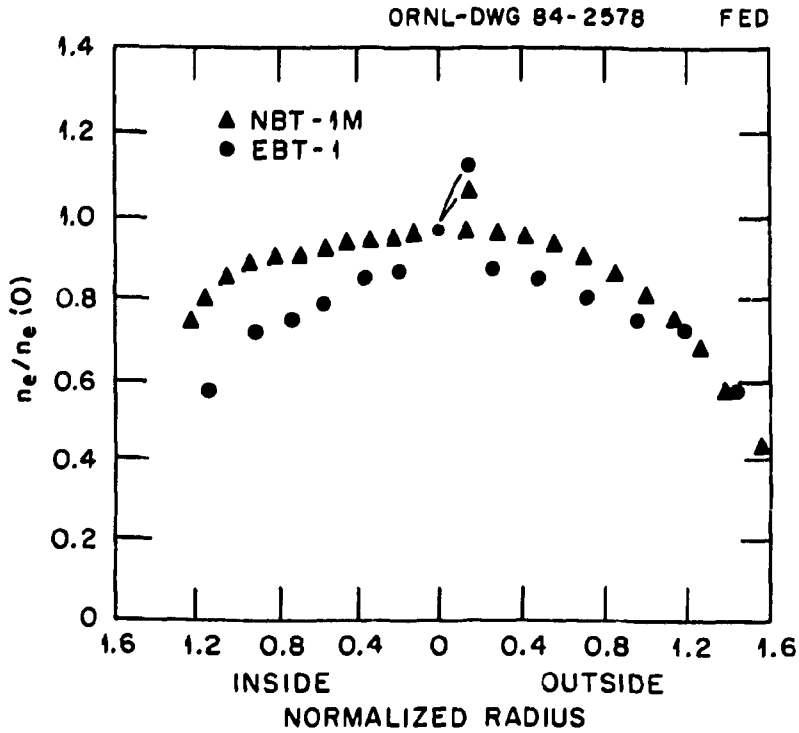

Fig. 7. Comparison of EBT-1 and NBT-1M density profiles at $p_o = 3 \times 10^{-5}$ torr. Applied microwave powers are the same as in Fig. 5.

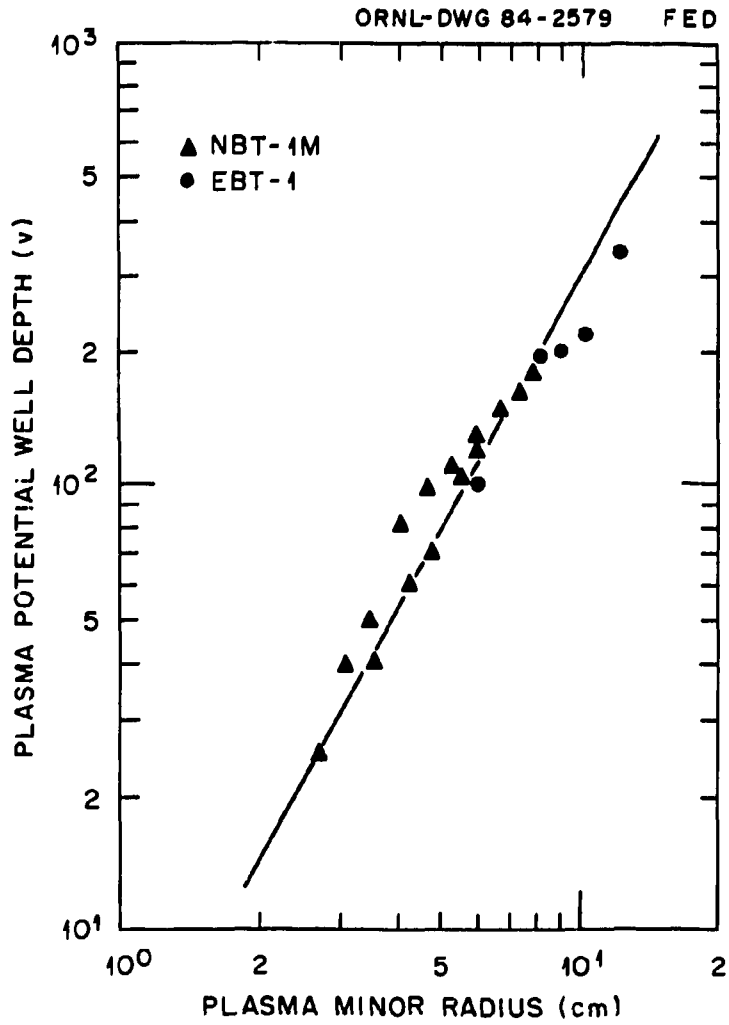

Fig. 8. Plasma well depth as a function of minor radius (i.e., ring diameter) for EBT-1 and NBT-1M.

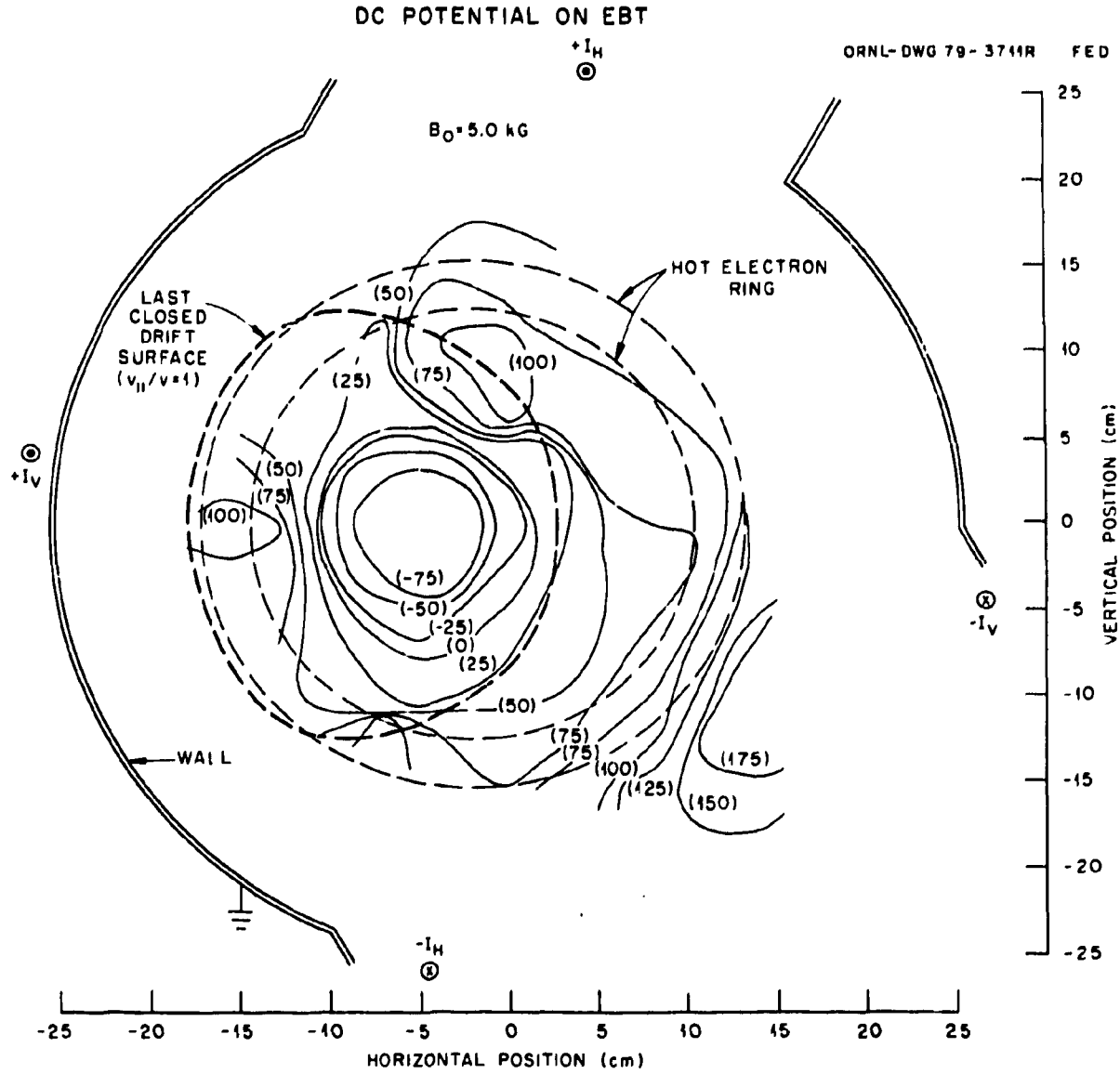

Fig. 9. Plasma potential contours in EBT-1; p_o = 1.85 x 10^{-5} torr, and P_μ(18 GHz) = 50 kW, P_μ(10.6 GHz) = 3 kW.

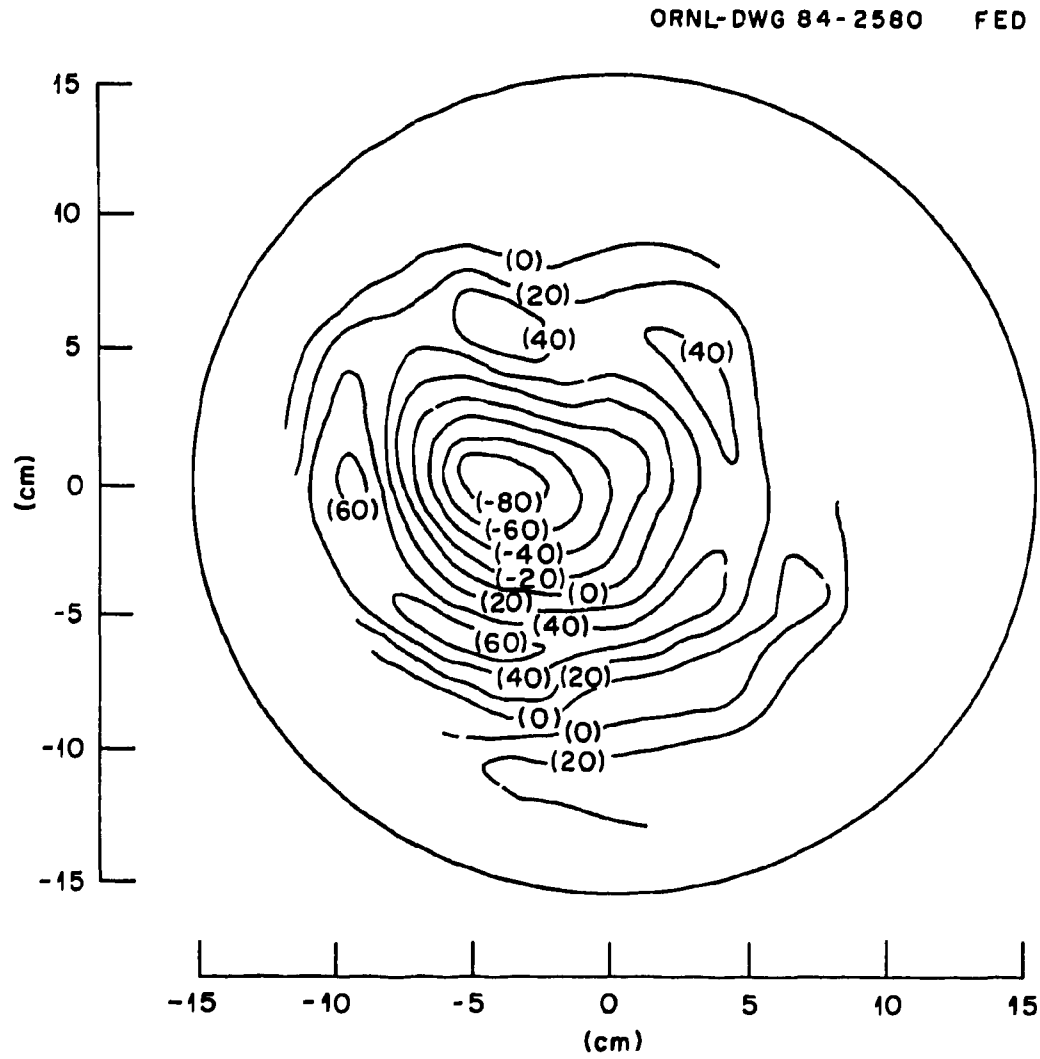

Fig. 10. Plasma potential contours in NBT-1M; p_o = 1.4 x 10^{-5} torr, and P_μ(18 GHz) = 30 kW.

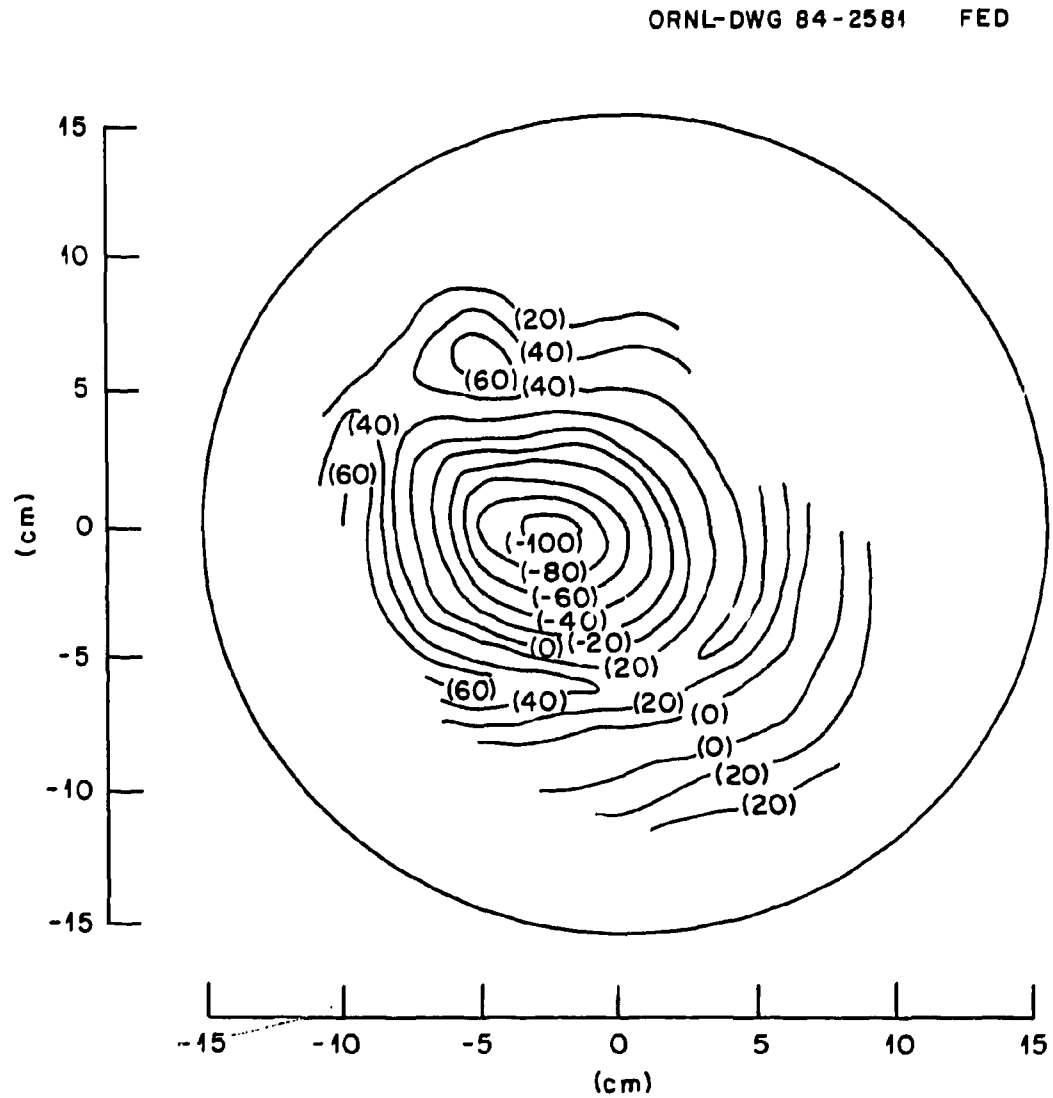

Fig. 11. Plasma potential contours in NBT-1M; p_o = 1.5 x 10^{-5} torr, and P_μ(18 GHz) = 30 kW, P_μ(8.5 GHz) = 15 kW.

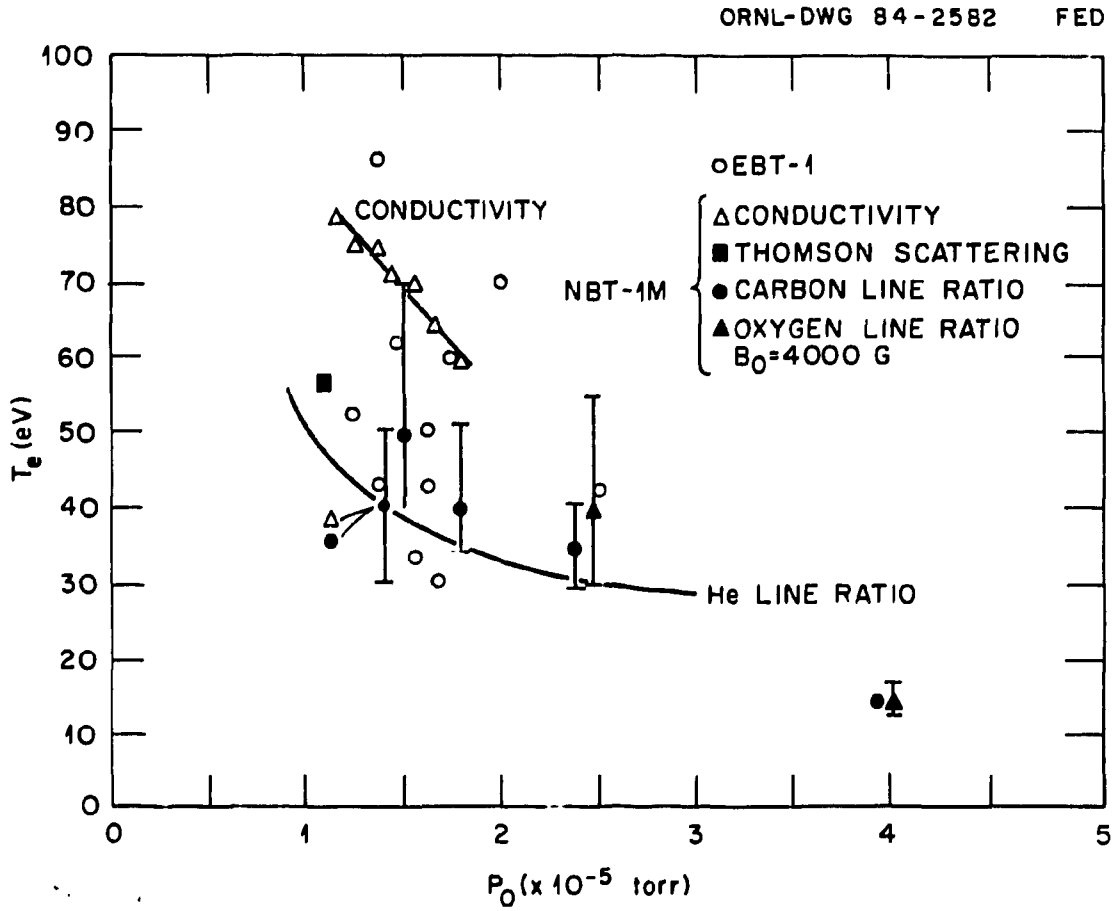

Fig. 12. Electron temperature as a function of pressure for NBT-1M at P_μ(18 GHz) = 30 kW and for EBT-1 with P_μ(18 GHz) = 40 kW and P_μ(10.6 GHz) = 6-10 kW.

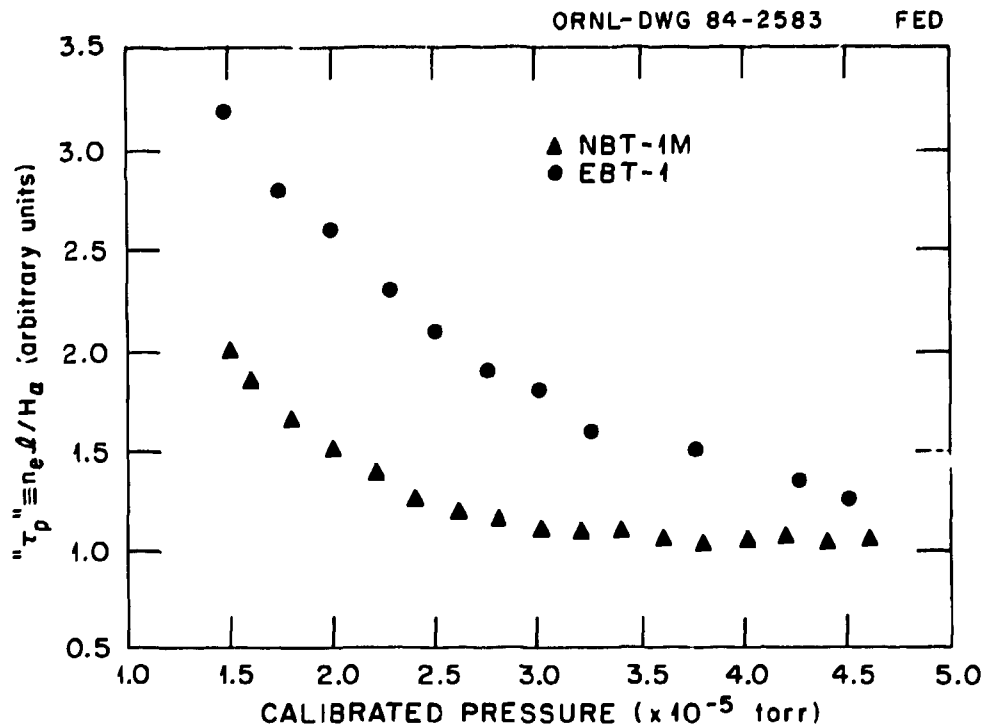

Fig. 13. Particle confinement time (uncalibrated) vs pressure for EBT-1 and NBT-1M; P_μ = 30 kW in NBT-1M, and P_μ = 45 kW in EBT-1.

ORNL/TM-9128
Dist. Category UC-20 f,g

INTERNAL DISTRIBUTION

1. F. W. Baity
2. L. A. Berry
3. T. S. Bigelow
4. N. B. Bryson
5. J. A. Cobble
6–10. R. J. Colchin
11. W. A. Davis
12. A. M. El-Nadi
13–17. J. C. Glowienka
18. G. R. Haste
19. D. L. Hillis
20. S. Hiroe
21. O. V. Jett
22. D. A. Rasmussen
23. J. Sheffield
24. L. Solensten
25. D. W. Swain
26. T. Uckan
27. J. K. Johnson
28–29. Laboratory Records Department
30. Laboratory Records, ORNL-RC
31. Document Reference Section
32. Central Research Library
33. Fusion Energy Division Library
34. Fusion Energy Division Publications Office
35. ORNL Patent Office

EXTERNAL DISTRIBUTION

36. W. B. Ard, McDonnell Douglas Corp., Bldg. 107, P.O. Box 516, St. Louis, MO 63166
37. H. L. Berk, University of Texas, Institute of Fusion Studies, Robert L. Moore Hall, Rm. 11-218, Austin, TX 78712
38. R. A. Dandl, Applied Microwave Plasma Concepts, 2210 Encinitas Blvd., Encinitas, CA 92024
39. A. J. Favale, Grumman Aerospace Corp., South Oyster Bay Rd., P.O. Box 31, Bethpage, NY 11714
40. N. A. Davies, U.S. Department of Energy, Office of Fusion Energy, Office of Energy Research, Mail Station G-256, Washington, DC 20545
41. G. G. Gibson, Westinghouse Electric Corp., Fusion Power Systems, Dept. C., P.O. Box 10864, Pittsburgh, PA 15236
42. H. Ikegami, Institute of Plasma Physics, Nagoya University, Nagoya 464, Japan
43. N. A. Krall, Jaycor, 11011 Torreyana Rd., P.O. Box 85154, San Diego, CA 92138
44. J. Lassoon, TRW Defense and Space Systems, 1 Space Park, Bldg. R-1, Rm 1078, Redondo Beach, CA 92078
45. N. H. Lazar, TRW Defense and Space Systems, 1 Space Park, Bldg. R-1, Rm. 1078, Redondo Beach, CA 92078
46. J. B. McBride, Science Applications, Inc., 1200 Prospect Street, P.O. Box 2351, La Jolla, CA 92037
47. F. L. Ribe, 319 Benson Hall BF 10, Department of Nuclear Engineering, University of Washington, Seattle, WA 98195
48. J. M. Turner, U.S. Department of Energy, Office of Fusion Energy, Office of Energy Research, Mail Station G-256, Washington, DC 20545

49. H. Weitzner, New York University, Courant Institute of Mathematical Sciences, 251 Mercer Street, New York, NY 10012
50. R. L. Hickok, Rensselaer Polytechnic Institute, ESE Department, Engineering Building, Troy, NY 12181
51. J. D. Callen, Department of Nuclear Engineering, University of Wisconsin, Madison, WI 53706
52. R. W. Conn, Department of Chemical, Nuclear, and Thermal Engineering, University of California, Los Angeles, CA 90024
53. S. O. Dean, Director, Fusion Energy Development, Science Applications, Inc., 2 Professional Drive, Gaithersburg, MD 20760
54. H. K. Forsen, Bechtel Group, Inc., Research Engineering, P.O. Box 3965, San Francisco, CA 94105
55. R. W. Gould, Department of Applied Physics, California Institute of Technology, Pasadena, CA 91125
56. F. M. Bieniosek, McDonnell Douglas Astronautics Company, 969 Executive Parkway, Bellerive Office Center, Creve Coeur, MO 63141
57. M. Fujiwara, Institute of Plasma Physics, Nagoya University, Nagoya 464, Japan
58. W. M. Stacey, Jr., School of Nuclear Engineering, Georgia Institute of Technology, Atlanta, GA 30332
59. G. A. Eliseev, I. V. Kurchatov Institute of Atomic Energy, P.O. Box 3402, 123182 Moscow, U.S.S.R.
60. V. A. Glukhikh, Scientific-Research Institute of Electro-Physical Apparatus, 188631 Leningrad, U.S.S.R.
61. I. Spighel, Lebedev Physical Institute, Leninsky Prospect 53, 117924 Moscow, U.S.S.R.
62. D. D. Ryutov, Institute of Nuclear Physics, Siberian Branch of the Academy of Sciencies of the U.S.S.R., Sovetskaya St. 5, 630090 Novosibirsk, U.S.S.R.
63. V. T. Tolok, Kharkov Physical-Technical Institute, Academical St. 1, 310108 Kharkov, U.S.S.R.
64. R. Varma, Physical Research Laboratory, Navrangpura, Ahmedabad, India
65. Bibliothek, Max-Planck-Institut fur Plasmaphysik, D-8046 Garching bei Munchen, Federal Republic of Germany
66. Bibliothek, Institut fur Plasmaphysik, KFA, Postfach 1913, D-5170 Julich, Federal Republic of Germany
67. Bibliotheque, Centre de Recherches en Physique des Plasmas, 21 Avenue des Bains, 1007 Lausanne, Switzerland
68. Bibliotheque, Service du Confinement des Plasmas, CEA, B.P. 6, 92 Fontenay-aux-Roses (Seine), France
69. Documentation S.I.G.N., Departement de la Physique du Plasma et de la Fusion Controlee, Centre d'Etudes Nucleaires, B.P. No. 85, Centre du Tri, 38041 Cedex, Grenoble, France
70. Library, Culham Laboratory, UKAEA, Abingdon, Oxfordshire, OX14 3DB, England
71. Library, FOM Institut voor Plasma-Fysica, Rijnhuizen, Jutphaas, The Netherlands
72. Library, Institute of Physics, Academia Sinica, Beijing, Peoples Republic of China
73. Library, Institute of Plasma Physics, Nagoya University, Nagoya 464, Japan
74. Library, International Centre for Theoretical Physics, Trieste, Italy
75. Library, Laboratorio Gas Ionizzati, Frascati, Italy
76. Library, Plasma Physics Laboratory, Kyoto University, Gokasho Uji, Kyoto, Japan

77. Plasma Research Laboratory, Australian National University, P.O. Box 4, Canberra, A.C.T. 2000, Australia
78. Thermonuclear Library, Japan Atomic Energy Research Institute, Tokai, Naka, Ibaraki, Japan
79. J. Barter, Lawrence Livermore National Laboratory, University of California, P.O. Box 808, Livermore, CA 94550
80. D. G. McAlees, Exxon Nuclear Company, Inc., 777 106th Avenue, N.E., Bellevue, WA 98009
81. P. J. Reardon, Princeton Plasma Physics Laboratory, P.O. Box 451, Princeton, NJ 08544
82. Office of the Assistant Manager for Energy Research and Development, Department of Energy, Oak Ridge Operations, P.O. Box E, Oak Ridge, TN 37830

83-290. Given distribution as shown in TID-4500, Magnetic Fusion Energy (Category Distribution UC-20 f,g: Experimental Plasma Physics, Theoretical Plasma Physics)